Electronic Supplementary Material (ESI) for Inorganic Chemistry Frontiers.

Supporting Information

Bimetallic CoZn Metal-Organic-Framework Derived CoZnS@NSC Co-Catalyst Loaded on g-C_3N_4 for Significantly Augmented Photocatalytic H_2 Evolution

Xiao-Jie Lu,‡[a] Ikram Ullah,‡[a] Jing-Han Li,[a] Shuai Chen,[a] Cheng-Zong Yuan,[b] and An-Wu Xu[a]*

[a]Division of Nanomaterials and Chemistry, Hefei National Research Center for Physical Sciences at the Microscale, University of Science and Technology of China, Hefei, Anhui 230026, P. R. China.

[b]School of Rare Earths, University of Science and Technology of China, Hefei, Anhui 230026, P. R. China.

‡These authors contributed equally to this work.

*Corresponding Authors:
An-Wu Xu; anwuxu@ustc.edu.cn

Experimental Section

1. Materials

The primary reagents used in this study, including $Co(NO_3)_26H_2O$ (≥ 99%), $Zn(NO_3)_2·6H_2O$ (≥ 98%), L-cysteine (≥ 98.5%), methanol (≥ 99.9%), urea (≥ 99%), and triethanolamine (TEOA, ≥ 99%), were purchased from Sinopharm Chemical Reagent Co., Ltd. 2-methylimidazole (≥ 99.8%) was bought from Sigma-Aldrich Chemicals. All of the above chemicals were used as purchased without further purification. Moreover, the deionized water used in all experiments with a resistivity of 18.2 MΩ at 25 ℃, was purified through Direct-Q 3 UV water purification system (Millipore Corp., France).

2. Characterization

Thermogravimetric analysis (TGA) was performed using a NETZSCH TG 209 F1 Libra TGA analyzer at a heating rate of 10 ℃ min^{-1} with α-Al_2O_3 as the reference. Powder X-ray diffraction (XRD) patterns of samples were recorded on a TTR-III theta rotating anode X-ray diffractometer operating at 40 kV voltage and 200 mA current with Cu Kα radiation (λ = 1.54187 Å) in all cases. Scanning electron microscopy (SEM) images were obtained using a GeminiSEM 450 microscope. The transmission electron microscopy (TEM) images were obtained by transmission electron microscopy (TEM), using a H-7650 HITACHI microscope with 100 kV accelerating voltage. The high-resolution TEM (HRTEM) images, high-angle annular dark-field scanning transmission electron microscopy (HAADF-STEM) images, and energy dispersive X-ray spectroscopy (EDX) elemental mapping were executed on an FEI Talos F200X field emission high-resolution transmission electron microscope at 200 kV accelerating voltage. Aberration-corrected HAADF-STEM (AC HAADF-STEM) imaging single atoms samples was performed on an FEI Themis Z

high-resolution transmission electron microscope with 200 kV. The nitrogen adsorption-desorption isotherms with Brunauer-Emmett-Teller (BET) specific surface area measurements were measured with a Micromeritics ASAP 2020 apparatus. The X-ray photoelectron spectroscopy (XPS) and valence band X-ray photoelectron spectra (VBXPS) were collected on a scanning X-ray microprobe (Thermo ESCALAB 250Xi) that used Al Ka radiation of 1486.6 eV and the C1s peak at 284.8 eV as an internal standard. Ultraviolet photoelectron spectroscopy (UPS) of the samples were investigated by a Thermo ESCALAB 250Xi analyzer having a monochromatic HeI light source (21.22 eV). The UV–vis diffuse reflectance spectra (DRS) of the obtained photocatalysts were obtained using a Shimadzu 3700 DUV UV-vis spectrometer equipped with a diffuse reflectance accessory. The spectra were recorded with $BaSO_4$ as the reflectance standard reference. The steady-state photoluminescence (PL) spectroscopy measurements were measured with a Hitachi F-7000 fluorescence spectrophotometer under an incident light of 370 nm. The time-resolved photoluminescence (TRPL) decay curves were collected on a Laser Strobe time-resolved spectrofluorometer (Photon Technology International (Canada) Inc.) with a GL-302 high-resolution dye laser (lifetimes 100 ps to 50 ms, excited by a nitrogen laser), a USHIO xenon lamp source and a 914-photomultiplier detection system.

3. Photoelectrochemical measurements

The photoelectrochemical measurements of the photocatalyst were carried out on an electrochemical workstation (CHI 760E, Shanghai Chenhua Limited, China) based on a standard three-electrode system consisting of a catalysts-coated fluorine-tin oxide (FTO) glass as the work electrode, a platinum wire as the counter electrode, a saturated Ag/AgCl (saturated in KCl solution) as the reference electrode, and Na_2SO_4 (0.5 M, 100 mL) as the electrolyte solution. To prepare a working electrode, 2 mg of catalyst was dispersed in 1 mL ethanol containing 10 μL Nafion (5

wt%, D520, DuPont Inc., USA) by ultrasonication. The resulting dispersion was then loaded onto the 1 × 2 cm^2 FTO glass (an effective area of about 1.0 cm^2) and dried naturally at room temperature. The electrochemical impedance spectroscopy (EIS) Nyquist plots were collected with frequencies ranging from 10 mHz to 100 kHz under visible light and a bias of -0.2 V. The transient photocurrent responses (TPR) were measured for each switch turn-on/turn-off event (300 W Xe lamp) under a bias voltage of 0.5 V.

4. Photocatalytic experiments

As shown in Fig. S11, Photocatalytic water splitting experiments for H_2 generation were performed in a Pyrex top-irradiated quartz vessel connected to a glass-enclosed system with a 300 W Xe lamp (CEL-HXF300-T3, Beijing China Education Au-light Technology Co., Ltd.) as the light source equipping with an optical UV cut-off filter to control the wavelength of incident light ($\lambda \geq 400$ nm). The spectrum of a CEL-HXE300-T3 Xe lamp ($\lambda \geq 400$ nm) is shown in Fig. S12. Typically, 50 mg of photocatalyst powder was added to an aqueous solution (100 mL) of triethanolamine (10 vol %, as a sacrificial reagent). Prior to exposure to light, the reactional system was evacuated with a vacuum pump for 0.5 h in the dark with continuous stirring to remove air, ensure anaerobic conditions in the reaction system, and reach adsorption-desorption equilibrium. In addition, the temperature of the suspension was maintained at a constant 10 ℃ throughout the photocatalytic reaction using a cooling water circulator, and the double-layered Pyrex reactor was continuously stirred. The amount of H_2 evolved was sampled every 1 h by an online automated flow-injection apparatus and then examined by an online gas chromatography (GC1120 system, Shanghai Sunny Hengping Limited) equipped with a thermal conductivity detector (TCD), using Argon as the carrier gas. After the reaction, the photocatalyst was separated from the reaction

solution for further use and characterization. For stability testing, the system was subjected to a 20 h recycling experiment with intermittent evacuation every 4 h and repeated 5 times.

The apparent quantum yield (AQY) of H_2 evolution was assayed by irradiating a mixture of 100 ml of 10% TEOA solution containing 50 mg CoZnS@NSC-15/g-C_3N_4 photocatalyst. The procedure was similar to that of the H_2 evolution test, except that the irradiation was supplied by monochromatic light of the 300 W Xe lamp equipped with different bandpass filters of λ = 400, 420, 450, 500, 550, and 600 ± 5 nm. The AQE value was calculated by the following equation:

$$AQY\ (\%) = \frac{Number\ of\ evolved\ H_2\ molecules \times 2}{Number\ of\ incident\ photons} \times 100\%$$

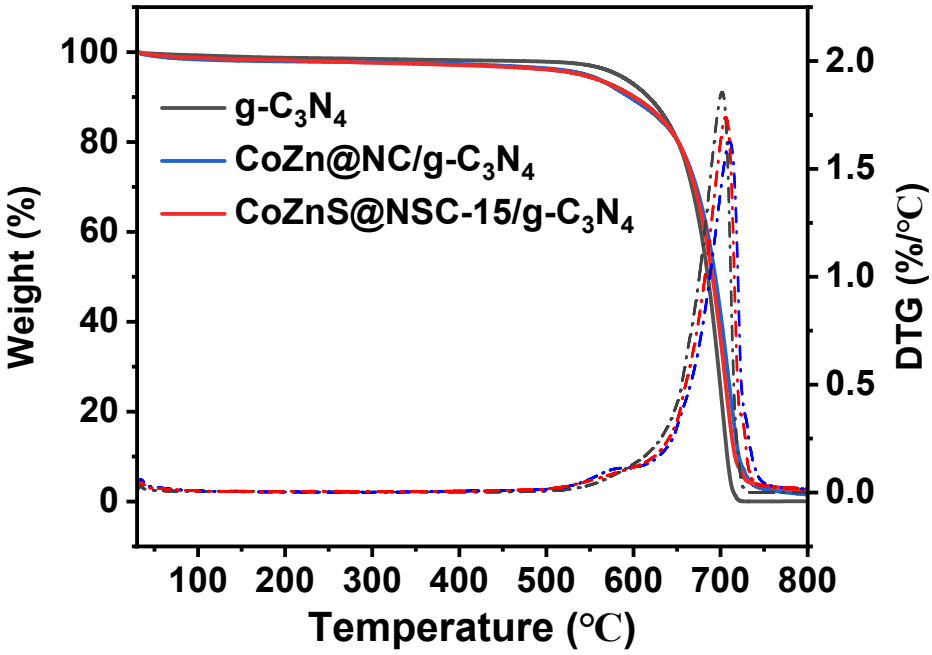

Fig. S1 TGA curves of g-C_3N_4, CoZn@NC/g-C_3N_4, and CoZnS@NSC-15/g-C_3N_4 at a ramping rate of 10 °C min^{-1}.

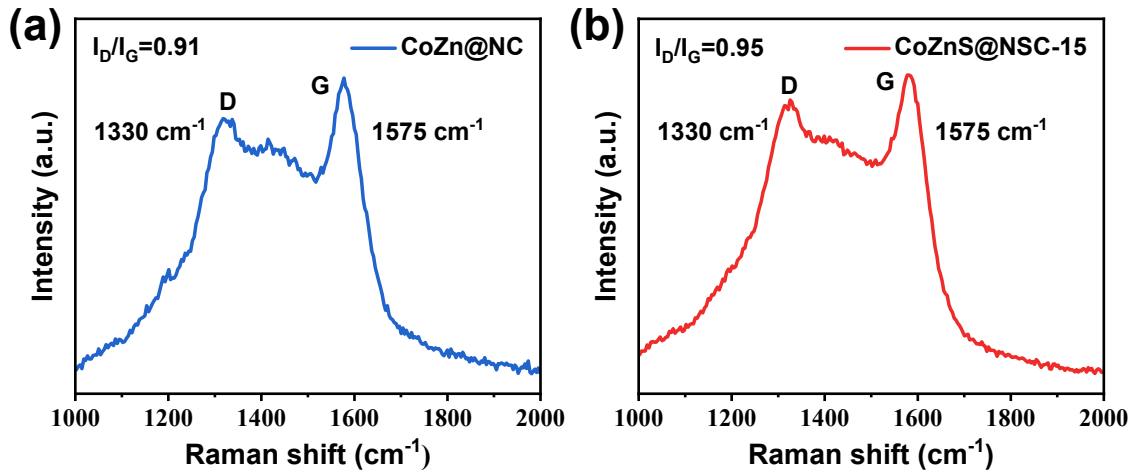

Fig. S2 The Raman spectrums of CoZn@NC and CoZnS@NSC-15 composites.

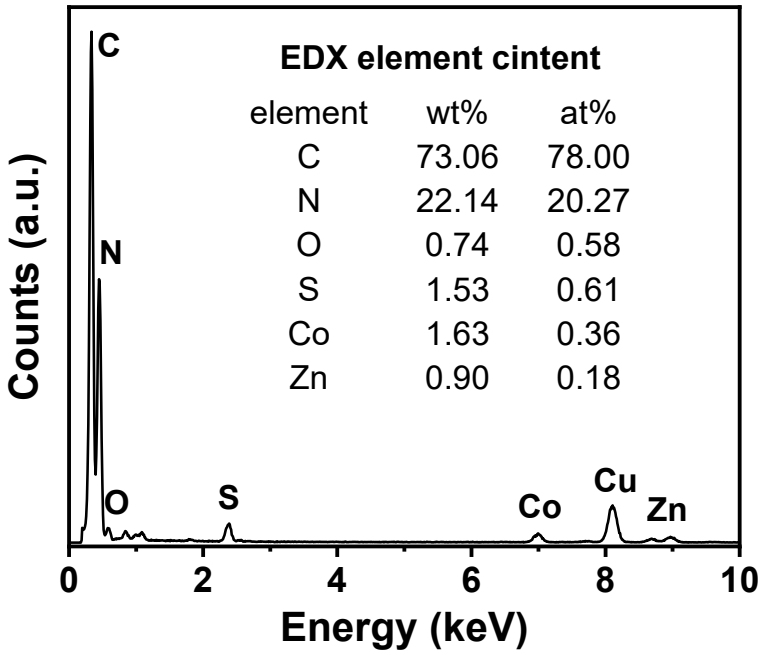

Fig. S3 EDX spectrum and elemental concentrations of CoZnS@NSC-15/g-C_3N_4 photocatalysts.

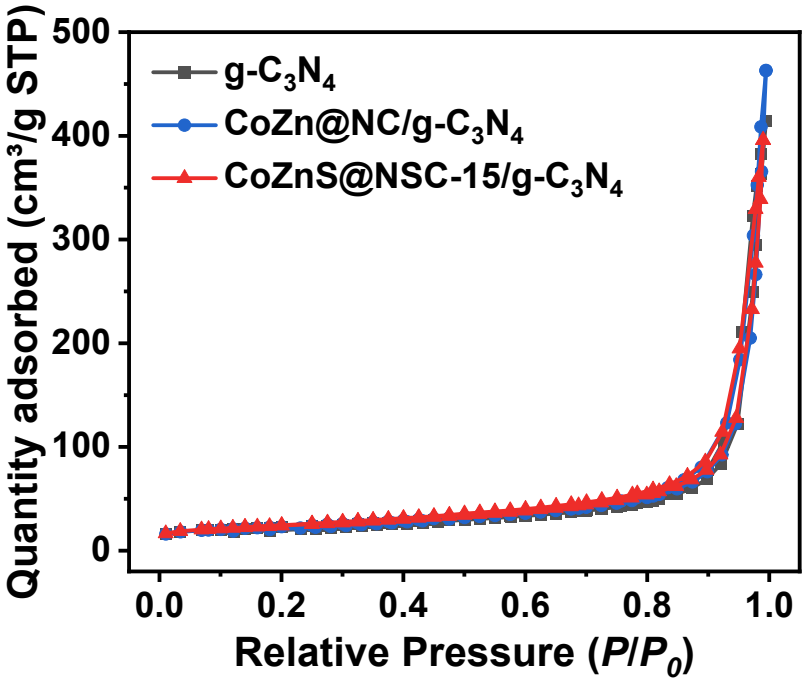

Fig. S4 N_2 adsorption-desorption isotherms of g-C_3N_4, CoZn@NC/g-C_3N_4, and CoZnS@NSC-15/g-C_3N_4 photocatalysts.

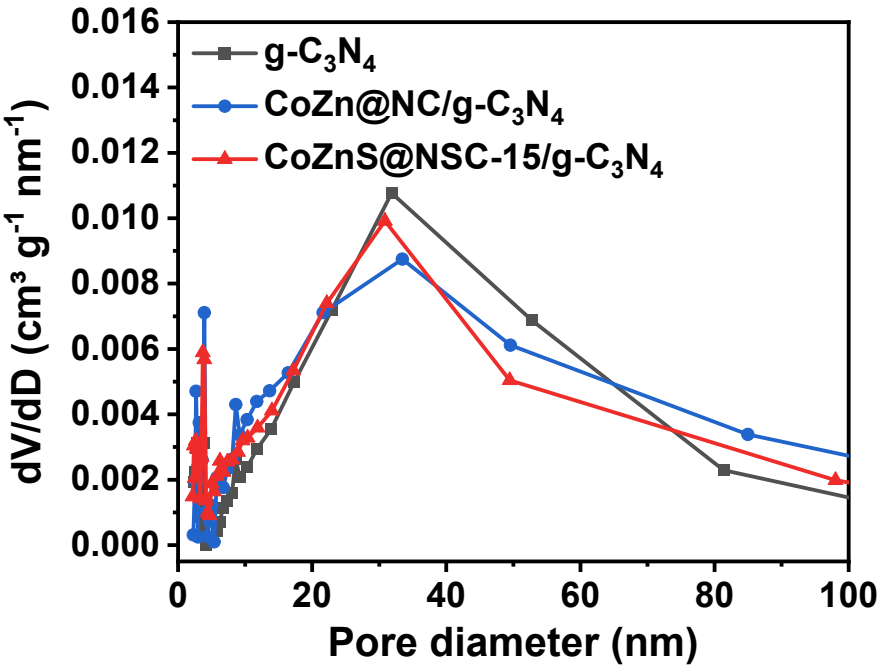

Fig. S5 Pore size distribution calculated by the BJH method of g-C_3N_4, CoZn@NC/g-C_3N_4, and CoZnS@NSC-15/g-C_3N_4 photocatalysts.

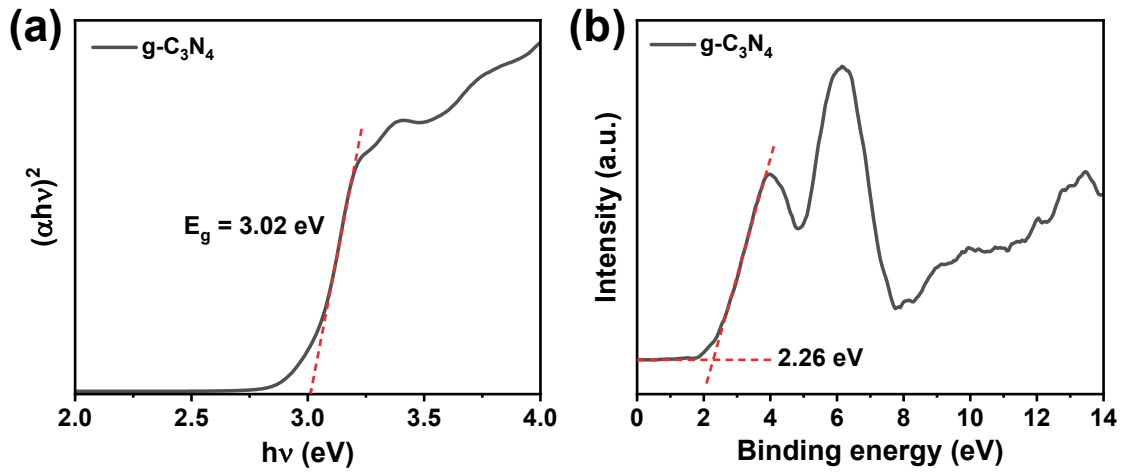

Fig. S6 (a) Tauc plots and (b) VB XPS spectra of g-C_3N_4.

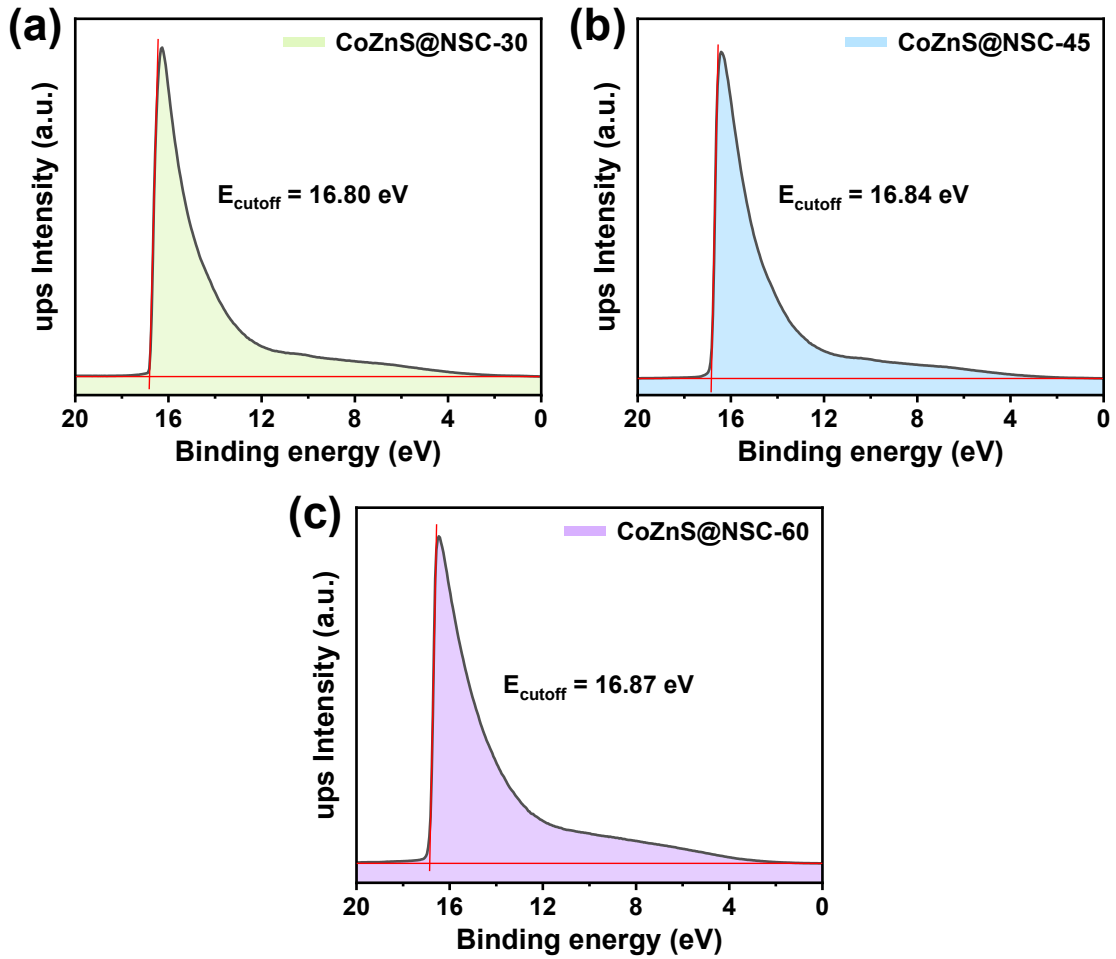

Fig. S7 Onset level of secondary electron cutoff of UPS spectrum of (a) CoZnS@NSC-30, (b) CoZnS@NSC-45, and (c) CoZnS@NSC-60 nanoparticles.

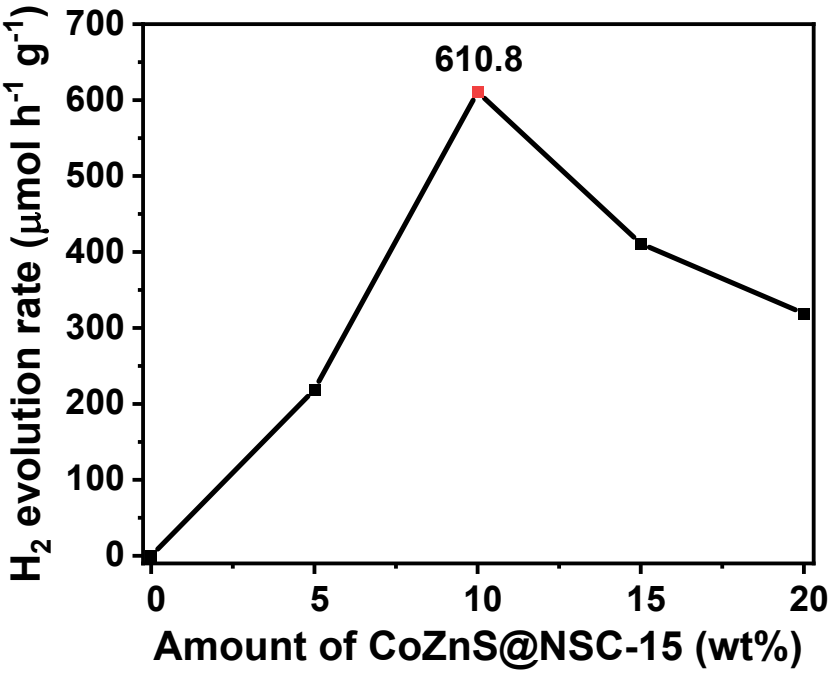

Fig. S8 Influence of CoZnS@NSC-15 loading content on photocatalytic H_2 evolution of ConZnS@NSC-15/g-C_3N_4 at $\lambda \geq 400$ nm.

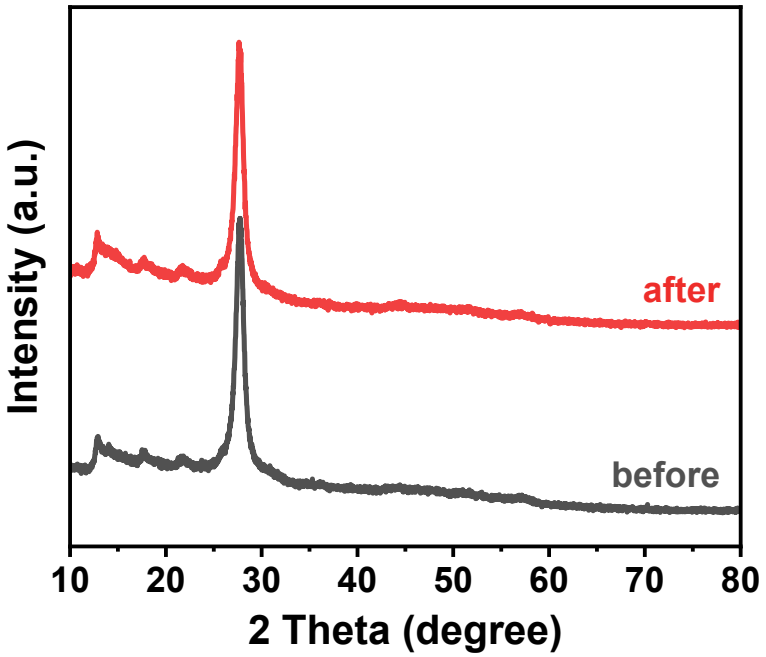

Fig. S9 The XRD patterns of ConZnS@NSC-15/g-C_3N_4 photocatalyst before and after cycle test.

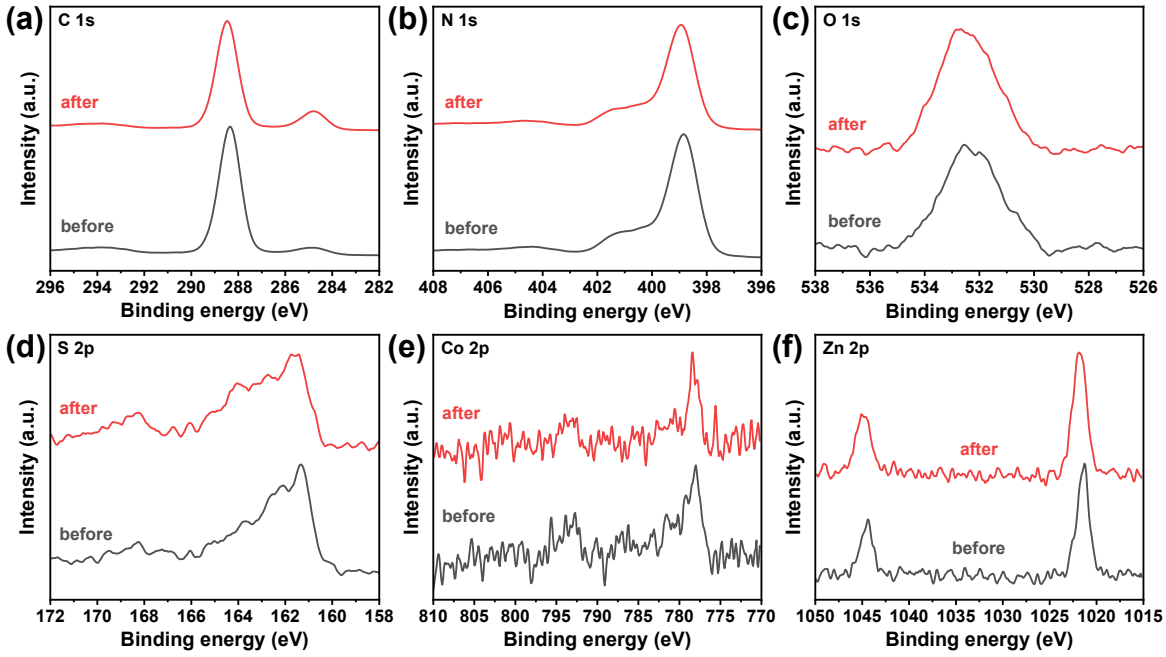

Fig. S10 High-resolution XPS spectra of (a) C 1s, (b) N1s, (c) O1s, (d) S 2p, (e) Co 2p, and (f) Zn 2p for ConZnS@NSC-15/g-C_3N_4 photocatalyst before and after cycle test.

Fig. S11 Photocatalysis equipment picture for the photocatalytic hydrogen evolution test.

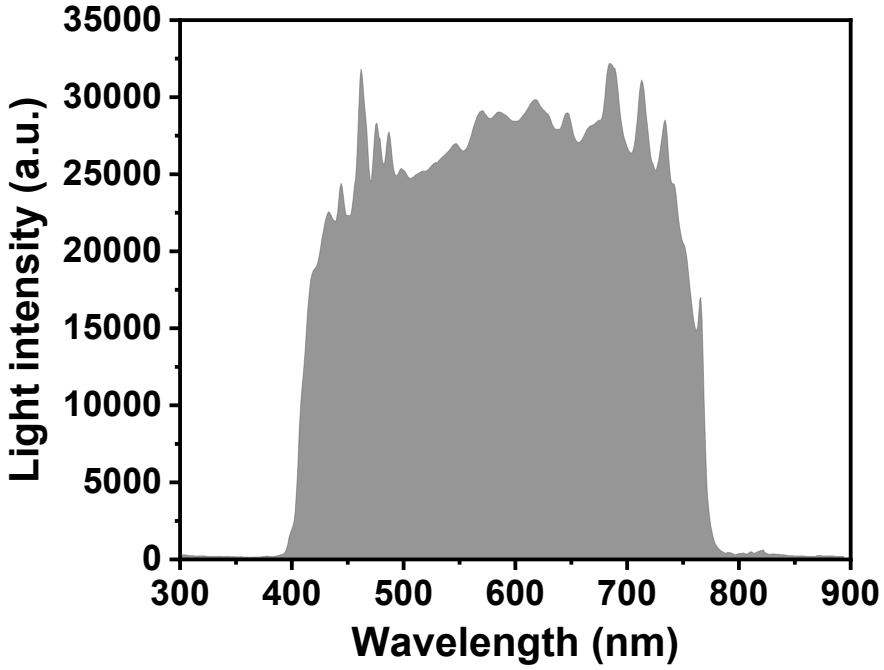

Fig. S12 Spectrum of the power as a function of wavelength for a CEL-HXE300 Xe lamp equipped with an optical UV cut-off filter ($\lambda \geq 400$ nm).

Table S1. BET specific surface areas, average pore diameter and total pore volumes of g-C_3N_4, CoZn@NC/g-C_3N_4, and CoZnS@NSC-15/g-C_3N_4.

Samples	S_{BET} (m^2 g^{-1})	V_{pore} (cm^3 g^{-1})	D_{pore} (nm)
g-C_3N_4	76	0.64	35.36
CoZn@NC/g-C_3N_4	80	0.71	36.59
CoZnS@NSC-15/g-C_3N_4	83	0.61	30.75

Table S2. Kinetic analysis of emission decay for g-C_3N_4, CoZn@NC/g-C_3N_4, and CoZnS@NSC-15/g-C_3N_4.

Samples	τ_1 (ns)	Rel (%)	τ_2 (ns)	Rel (%)	τ_3 (ns)	Rel (%)	τ (ns)	X^2
g-C_3N_4	3.81	52.83	15.14	27.48	1.08	19.70	2.95	1.15
CoZn@NC/g-C_3N_4	3.13	51.34	13.42	39.12	0.79	19.54	2.42	1.09
CoZnS@NSC-15/g-C_3N_4	2.52	49.04	11.18	28.52	0.58	22.44	1.65	1.16

Table S3. Comparison of our study highest H_2 evolution rate with various co-catalyst modified g-C_3N_4-based photocatalysts.

Co-catalyst	Light Source	Conditions	H_2 evolution rate ($\mu mol\ h^{-1}\ g^{-1}$)	Ref
10% CoZnS@NSC-15	300W Xe lamp ($\lambda \geq 400$ nm)	10 vol% TEOA	**610.8**	**This work**
2% Mo-Mo_2C	300W Xe lamp ($\lambda \geq 420$ nm)	10 vol% TEOA	219.7	1
4% CoNi	300W Xe lamp ($\lambda \geq 420$ nm)	15 vol% Lactic acid	354.4	2
CB-$Co_{1.4}Ni_{0.6}P$	300W Xe lamp ($\lambda \geq 420$ nm)	15 vol% TEOA	403.0	3
NiS	300W Xe lamp ($\lambda \geq 420$ nm)	10 vol% TEOA	244.0	4
1% Ni_2P-1.5%MoS_2	300W Xe lamp ($\lambda \geq 400$ nm)	15 vol% TEOA	532.4	5
3% CoP/Co@NPC-15	300W Xe lamp ($\lambda \geq 420$ nm)	15 vol% TEOA	374.1	6
3% Ni_2P	300W Xe lamp ($\lambda \geq 420$ nm)	10 vol% TEOA	128.7	7
40% CNCNT	300W Xe lamp	10 vol% TEOA	1208	8
2% $CoMoS_2$/ 0.5 % rGO	300W Xe lamp ($\lambda \geq 400$ nm)	20 vol% TEOA	684	9

References

1. J. Dong, Y. Shi, C. Huang, Q. Wu, T. Zeng and W. Yao, A New and stable Mo-Mo_2C modified g-C_3N_4 photocatalyst for efficient visible light photocatalytic H_2 production, *Appl. Catal. B: Environ.*, 2019, **243**, 27-35.

2. C. Lu, E. Wu, C. Li, W. Dou, Y. Lian, Y. Liang, X. Xiang and H. Wang, CoNi bimetallic alloy cocatalyst-modified g-C_3N_4 nanosheets for efficient photocatalytic hydrogen production, *Journal of Physics and Chemistry of Solids*, 2021, **158**, 110228.

3. R. Shen, W. Liu, D. Ren, J. Xie and X. Li, $Co_{1.4}Ni_{0.6}P$ cocatalysts modified metallic carbon black/g-C_3N_4 nanosheet Schottky heterojunctions for active and durable photocatalytic H_2 production, *Appl. Surf. Sci.*, 2019, **466**, 393-400.

4. M. Wang, J. Cheng, X. Wang, X. Hong, J. Fan and H. Yu, Sulfur-mediated photodeposition synthesis of NiS cocatalyst for boosting H_2-evolution performance of g-C_3N_4 photocatalyst, *Chin. J. Catal.*, 2021, **42**, 37-45.

5. X. Lu, J. Xie, X. Chen and X. Li, Engineering MPx (M = Fe, Co or Ni) interface electron transfer channels for boosting photocatalytic H_2 evolution over g-C_3N_4/MoS_2 layered heterojunctions, *Appl. Catal. B: Environ.*, 2019, **252**, 250-259.

6. Q. Ji, L. Pan, J. Xu, C. Wang and L. Wang, Zeolitic Imidazolate Framework-67-Derived CoP/Co@N,P-Doped Carbon Nanoparticle Composites with Graphitic Carbon Nitride for Enhanced Photocatalytic Production of H_2 and H_2O_2, *ACS Appl. Nano Mater.*, 2020, **3**, 3558-3567.

7. Y. Xiao, Z. Wang, L. Li, Q. Gu, M. Xu, L. Zhu and X. Fu, Ball-milled Ni_2P/g-C_3N_4 for improved photocatalytic hydrogen production, *Int. J. Hydrogen Energy*, 2023, **48**, 15460-15472.

8. Q. Liu, C. Zeng, Z. Xie, L. Ai, Y. Liu, Q. Zhou, J. Jiang, H. Sun and S. Wang, Cobalt@nitrogen-doped bamboo-structured carbon nanotube to boost photocatalytic hydrogen evolution on carbon nitride, *Appl. Catal. B: Environ.*, 2019, **254**, 443-451.

9. X. Xu, Z. Si, L. Liu, Z. Wang, Z. Chen, R. Ran, Y. He and D. Weng, $CoMoS_2$/rGO/C_3N_4 ternary heterojunctions catalysts with high photocatalytic activity and stability for hydrogen evolution under visible light irradiation, *Appl. Surf. Sci.*, 2018, **435**, 1296-1306.